THE ASTROPHYSICAL JOURNAL, 184:493–516, 1973 September 1

HOT CNO-Ne CYCLE HYDROGEN BURNING. I. THERMONUCLEAR EVOLUTION AT CONSTANT TEMPERATURE AND DENSITY*

JEAN AUDOUZE†
California Institute of Technology, Pasadena, California
JAMES W. TRURAN
Belfer Graduate School of Science, Yeshiva University, New York, New York
AND
BARBARA A. ZIMMERMAN
California Institute of Technology, Pasadena, California
Received 1973 March 16; revised 1973 April 26

ABSTRACT

The relative concentrations of nuclei achieved in hydrogen burning on carbon, nitrogen, and oxygen at high temperatures are calculated as a function of time. Calculations have been performed for static burning conditions, for temperatures in the range $0.1 \leq T_9 \leq 1$ and densities $1 \leq \rho \leq 10^3$ g cm^{-3}. The Ne-Na cycle also operates under these high-temperature conditions. A network comprising 28 nuclei from ^{12}C to ^{25}Mg, related by 60 (p, γ), (p, α), (α, γ), (α, n), and positron decay reactions, has been used in this study. At higher temperatures the (p, γ) and (p, α) thermonuclear reaction rates are typically much faster than the positron decay rates, quite in contrast to the situation existing under the usual CNO bi-cycle burning conditions in stellar cores. This distinguishing feature leads to nucleosynthesis which differs significantly from that calculated at lower temperatures. Specifically, large enhancements of nuclei of masses $A = 15$, 17, 18, 19, 21, and 22 are found to occur at various stages of the burning at constant temperature (the stable nuclei on these isobars being ^{15}N, ^{17}O, ^{18}O, ^{19}F, ^{21}Ne, and ^{22}Ne). Under some conditions, ^{13}C/^{12}C ratios exceeding unity are achieved, in contrast to the ratio ^{13}C/^{12}C = 0.29 characteristic of equilibrium in the CNO bi-cycle at lower temperatures, $T \lesssim 70$ million degrees. The physical conditions determined to be most promising for nucleosynthesis provide insight as to possible sites for the formation of many of these lighter isotopes in astrophysical environments.

Subject headings: interiors, stellar — massive stars — nuclear reactions — abundances

I. INTRODUCTION

Since the discovery by Bethe (1939) and von Weizsäcker (1938) of the role of the CNO cycle in hydrogen burning occurring in the cores of massive main-sequence stars, a great deal of effort has been devoted to studies of the nuclear properties and astrophysical implications of this set of reactions. In previous works, Caughlan and Fowler (1962, 1964); Caughlan, Fowler, and Talbot (1964); and Caughlan (1965) have studied these reactions in the range of temperatures $10^{6\,\circ} < T \lesssim 10^{8\,\circ}$ K reached in the interior of these stars and in the hydrogen-burning shells of red giant stars. At these temperatures, it is now established that ^{12}C and ^{16}O are mainly transformed into ^{14}N as a consequence of the relatively slow rate of ^{14}N destruction. Stable but rarer isotopes like ^{13}C, ^{15}N, ^{17}O, and ^{18}O are not formed in sufficient amounts to account for their observed solar-system concentrations relative to ^{14}N.

The burning of hydrogen on CNO nuclei has also been investigated at temperatures

* Supported in part by the National Science Foundation [GP-28027, GP-36687X] at Caltech, and [GP-30289] at Yeshiva University.

† On leave from SEP CEN Saclay (France) and Observatoire de Meudon (France).

above 10^8 ° K in several recent contributions by Caughlan and Fowler (1972, 1973); Starrfield *et al.* (1972); and Starrfield, Sparks, and Truran (1973). For temperatures higher than 10^8 ° K substantial deviations from the usual CNO–Ne cycle patterns can occur. Hoyle and Fowler (1960) have noted, for instance, the importance of the reaction $^{13}N(p, \gamma)^{14}O$ which competes with $^{13}N(e^+\nu)^{13}C$ at such temperatures; Hoyle and Fowler (1965) have also shown that reactions like $^{14}O(\alpha, p)^{17}F$, $^{17}F(p, \gamma)^{18}Ne$, and $^{15}O(\alpha, \gamma)^{19}F$ can play an important role in the nuclear transformations occurring at $T > 5 \times 10^8$ ° K. Such temperatures may be achieved in hydrogen-rich material, for example, in nova explosions (Starrfield *et al.* 1972), in supermassive stars (Appenzeller and Fricke 1972), or in the envelopes of some supernovae. In contrast to burning at lower temperatures, the rates of nuclear reactions induced by protons and α-particles, which increase rapidly with temperature, typically exceed the β-decay rates under these conditions. The more abundant nuclei on shorter burning time scales (< 50–100 s) are thus those β-unstable nuclei which are not rapidly destroyed by (p, γ) or (p, α) reactions. The abundances resulting from this thermonuclear processing can differ substantially from the low-temperature case. In particular, nuclear species like ^{13}C, ^{14}N, ^{15}N, and ^{17}O which have an unstable isobaric parent of β lifetime $\gtrsim 50$ s can be enhanced in such situations.

In this paper, nuclear transformations induced by protons and α-particles involving nuclei from ^{12}C to ^{25}Mg have been studied for temperatures $0.1 \leq T_9 \leq 1$ (T_9 is the temperature in units 10^9 ° K) and densities $1 \leq \rho \leq 10^3$ g cm^{-3}. Calculations have been performed for constant temperature and density conditions only. The motivation for this investigation is provided by the following considerations. (1) The nuclear reaction rates, hence the character of the thermonuclear evolution, are strongly temperature dependent, and it is instructive to explore the consequences of this dependence without introducing the further complications that arise due to time variations of the physical conditions in hydrodynamic studies. (2) "Equilibrium" calculations such as those performed by Caughlan (1965) and Caughlan and Fowler (1972, 1973) at lower temperatures ($T_9 \lesssim 0.3$) are no longer applicable at higher temperatures, since the time scale required to approach equilibrium or steady-state burning conditions is often comparable to the hydrogen-burning time scale. (3) The temperature and density conditions we have explored are consistent with those we expect may be achieved in the envelopes of novae and supernovae or in the interiors of supermassive stars. From this study, it may therefore be possible to infer the basic thermonuclear burning patterns appropriate to these different astrophysical settings. The variations of abundances with time have been followed in detail in an attempt to determine the limiting temperature, density, and time-scale conditions consistent with the formation of nuclear species like ^{13}C, ^{15}N, ^{17}O, ^{18}O, ^{19}F, ^{21}Ne, and ^{22}Ne.

In § II the nuclear reaction network is defined, and the sources of the specific reaction rates used in this study are indicated. The need for further nuclear experiments and improved theoretical estimates of critical reaction rates is emphasized. The results obtained in these studies at constant temperature are presented and analyzed in § III. The conditions required for the synthesis of specific isotopes in this mass region are summarized (§ IV), and the implications of these results for nucleosynthesis in various astrophysical environments are discussed (§ V).

II. THERMONUCLEAR REACTION RATES AND REACTION NETWORK

The thermonuclear reaction network considered in this study is illustrated in figure 1. We have included all the important reactions induced by protons, α-particles neutrons, and photons [(p, γ), (α, p), (α, n), and (α, γ) reactions and their inverses] together with the weak interactions (positron decays) which can influence the abundances of nuclei from ^{12}C to ^{25}Mg at temperatures $0.1 \leq T_9 \leq 1$. To follow the behavior of the neutrons, we have included both the relevant (α, n) reactions and the

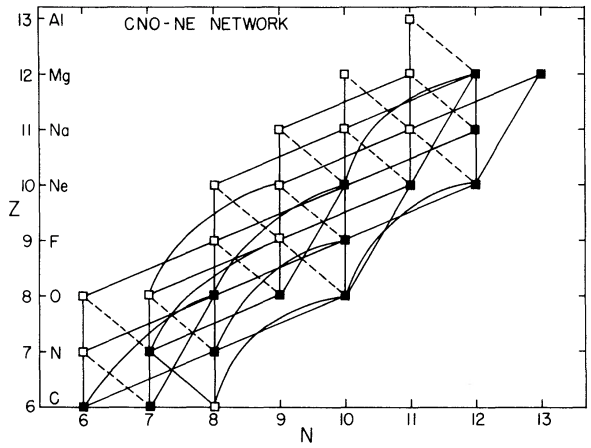

FIG. 1.—Illustration of the nuclear reaction network used in this study. The black dots represent the stable nuclei; the white dots represent the beta-unstable nuclei. They are linked by solid lines which represent the nuclear reactions (p, γ) (*vertical lines*), (α, n) (lines making a 25° angle with the abscissa), (α, p) or (p, α) (lines making a 60° angle with the abscissa), and (α, γ) (*curved lines*). The dashed lines represent the weak interactions (positron decays).

important $^{14}N(n, p)^{14}C$ reaction which provides the more stringent limitation on their number. The other (p, n) reactions have not been considered since they are more endothermic and they do not change the atomic mass of the target nucleus.

The rates of the reactions used in this study have been taken from three different sources. Table 1 indicates the specific reactions we have included and the source from which the rates have been taken. Nuclear experiments have provided improved rates for a number of these reactions that Fowler, Caughlan, and Zimmerman (1973) have incorporated in their latest analysis; however, many crucial rates have not been studied experimentally. In particular, the rates taken from the compilations of Wagoner (1969) and Wagoner, Fowler, and Hoyle (1967) represent theoretical estimates which, for reactions on these lighter nuclei, must be considered to have associated a substantial degree of uncertainty. This must be kept in mind for particularly important reactions like $^{14}O(\alpha, p)^{17}F$, $^{15}O(\alpha, \gamma)^{19}F$, or $^{17}F(p, \gamma)^{18}Ne$ which play a major role in the synthesis of nuclei of mass 17, 18, and 19.

The variation with time of the abundances of the nuclear species involved in the calculations is governed by a system of differential equations. These equations have been solved by standard numerical techniques (Scarborough 1966; see also Arnett and Truran 1969). Where not otherwise specified, the initial composition of the material has been assumed to be that of solar-system matter (Cameron 1968). The evolution has been followed for a range of temperature and density conditions for total times $\sim 10^5$ s; the interesting consequences for energy generation and nucleosynthesis are already apparent by this time, and we do not expect longer time scales to be consistent with such explosive hydrogen-burning conditions. For instance, the time scale of explosions in supermassive stars is a few times 10^4 s (Fricke 1973), and the light curves of the nova models studied by Starrfield *et al.* (1972, 1973) present a peak for times between 10^4 and 10^5 s.

III. THERMONUCLEAR EVOLUTION IN HIGH-TEMPERATURE HYDROGEN BURNING

The variations in abundance as a function of time resulting from the thermonuclear burning of matter comprised initially of a solar-system distribution[1] of

[1] Illustrative calculations performed for different initial compositions are summarized in the Appendix.

TABLE 1

TABLE OF THE REFERENCES OF THE NUCLEAR REACTION RATES

(p, γ) and (p, n) Reactions	(p, α) and (α, p) Reactions	(α, γ) and (α, n) Reactions	Weak Interactions with $\lambda(\beta^{\pm})$ in s^{-1}
$^{12}C(p, \gamma)^{13}C$ (FCZ)	$^{15}N(p, \alpha)^{12}C$ (FCZ)	$2\ ^{4}He(\alpha, \gamma)^{12}C$ (FCZ)	$n(\beta^{-})p$, 1.60(−3)
$^{13}C(p, \gamma)^{14}N$ (FCZ)	$^{13}N(\alpha, p)^{16}O$ (WFH)	$^{12}C(\alpha, \gamma)^{16}O$ (FCZ)	$^{13}N(\beta^{+})^{13}C$, 1.16(−3)
$^{14}C(p, \gamma)^{15}N$ (W)	$^{17}O(p, \alpha)^{14}N$ (FCZ)	$^{13}C(\alpha, n)^{16}O$ (FCZ)	$^{14}O(\beta^{+})^{14}N$, 9.80(−3)
$^{14}C(p, n)^{14}N$ (FCZ)	$^{18}O(p, \alpha)^{15}N$ (FCZ)	$^{14}C(\alpha, \gamma)^{18}O$ (W)	$^{15}O(\beta^{+})^{15}N$, 5.59(−3)
$^{13}N(p, \gamma)^{14}O$ (FCZ)	$^{14}O(\alpha, p)^{17}F$ (WFH)	$^{14}N(\alpha, \gamma)^{18}F$ (FCZ)	$^{17}F(\beta^{+})^{17}O$, 1.05(−2)
$^{14}N(p, \gamma)^{15}O$ (FCZ)	$^{18}F(p, \alpha)^{15}O$ (W)	$^{15}N(\alpha, \gamma)^{19}F$ (W)	$^{18}F(\beta^{+})^{18}O$, 1.05(−4)
$^{15}N(p, \gamma)^{16}O$ (FCZ)	$^{19}F(p, \alpha)^{16}O$ (FCZ)	$^{15}O(\alpha, \gamma)^{19}Ne$ (W)	$^{18}Ne(\beta^{+})^{18}F$, 4.74(−1)
$^{16}O(p, \gamma)^{17}F$ (FCZ)	$^{17}F(\alpha, p)^{20}Ne$ (WFH)	$^{17}O(\alpha, n)^{20}Ne$ (W)	$^{19}Ne(\beta^{+})^{19}F$, 3.85(−2)
$^{17}O(p, \gamma)^{18}F$ (FCZ)	$^{18}F(\alpha, p)^{21}Ne$ (W)	$^{18}O(\alpha, n)^{21}Ne$ (FCZ)	$^{20}Na(\beta^{+})^{20}Ne$, 1.70(0)
$^{18}O(p, \gamma)^{19}F$ (W)	$^{19}F(\alpha, p)^{22}Ne$ (W)	$^{20}Ne(\alpha, \gamma)^{24}Mg$ (FCZ)	$^{21}Na(\beta^{+})^{21}Ne$, 3.04(−2)
$^{17}F(p, \gamma)^{18}Ne$ (WFH)	$^{18}Ne(\alpha, p)^{21}Na$ (WFH)	$^{21}Ne(\alpha, n)^{24}Mg$ (FCZ)	$^{22}Na(\beta^{+})^{22}Ne$, 8.89(−9)
$^{18}F(p, \gamma)^{19}Ne$ (W)	$^{19}Ne(\alpha, p)^{22}Na$ (W)	$^{22}Ne(\alpha, n)^{25}Mg$ (FCZ)	$^{22}Mg(\beta^{+})^{22}Na$, 1.78(−1)
$^{19}F(p, \gamma)^{20}Ne$ (W)	$^{23}Na(p, \alpha)^{20}Ne$ (FCZ)		$^{23}Mg(\beta^{+})^{23}Na$, 5.80(−2)
$^{19}Ne(p, \gamma)^{20}Na$ (WFH)	$^{20}Na(\alpha, p)^{23}Mg$ (WFH)		$^{24}Al(\beta^{+})^{24}Mg$, 3.20(−1)
$^{20}Ne(p, \gamma)^{21}Na$ (FCZ)	$^{21}Na(\alpha, p)^{24}Mg$ (W)		
$^{21}Ne(p, \gamma)^{22}Na$ (W)	$^{22}Na(\alpha, p)^{25}Mg$ (W)		
$^{22}Ne(p, \gamma)^{23}Na$ (W)			
$^{21}Na(p, \gamma)^{22}Mg$ (WFH)			
$^{22}Na(p, \gamma)^{23}Mg$ (WFH)			
$^{23}Na(p, \gamma)^{24}Mg$ (FCZ)			
$^{23}Mg(p, \gamma)^{24}Al$ (WFH)			

SOURCE.—FCZ = Fowler, Caughlan, and Zimmerman 1973; W = Wagoner 1969; WFH = Wagoner, Fowler, and Hoyle 1967.

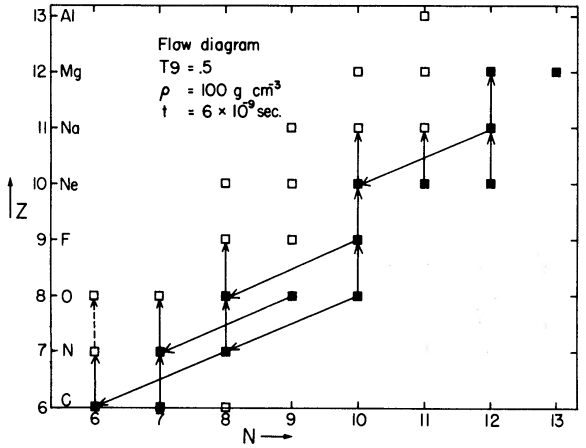

FIG. 2.—Flow diagram at $T_9 = 0.5$, $\rho = 100$ g cm^{-3}, and $t = 6 \times 10^{-9}$ s. At the beginning of the process the dominant reactions are the (p, γ) reactions and especially the (p, α) reactions induced on the stable nuclei.

abundances (Cameron 1968) are presented for densities from 1 to 1000 g cm^{-3} and temperatures $T_9 = 0.1$, 0.2, 0.5, and 1.0, respectively. Since the reaction rates, hence the thermonuclear evolution, are most strongly dependent on the temperature, we present the result of our investigation below as a function of this parameter. It will first be useful to note certain general characteristics of the patterns of nuclear transformations which dictate the production of interesting nuclei from ^{12}C to ^{25}Mg. For the temperature range considered here, $0.1 \leq T_9 \leq 1$, the general character of the nuclear transformations affecting the interesting nuclei from ^{12}C up to ^{25}Mg may be illustrated with the use of "flow diagrams."

Early in the thermonuclear processing history of hydrogen-rich matter exposed to these conditions, the character of the thermonuclear evolution is more or less the same independent of the temperature. The dominant reactions are (p, γ) and (p, α) reactions operating on stable nuclei (fig. 2), specifically: the proton-capture reactions $^{12}C(p, \gamma)^{13}N$, $^{13}C(p, \gamma)^{14}N$, $^{14}N(p, \gamma)^{15}O$, $^{15}N(p, \gamma)^{16}O$, $^{16}O(p, \gamma)^{17}F$, $^{18}O(p, \gamma)^{19}F$, $^{20}Ne(p, \gamma)^{21}Na$, $^{21}Ne(p, \gamma)^{22}Na$, $^{22}Ne(p, \gamma)^{23}Na$, $^{23}Na(p, \gamma)^{24}Mg$; and the (p, α) reactions $^{15}N(p, \alpha)^{12}C$, $^{17}O(p, \alpha)^{14}N$, $^{18}O(p, \alpha)^{15}N$, $^{19}F(p, \alpha)^{16}O$, and $^{23}Na(p, \alpha)^{20}Ne$. The cyclic behavior typical of CNO burning is not apparent on these short time scales, since it requires significant contributions from the relatively long-lived positron decays of proton-rich isotopes. However, one can initially expect a rapid depletion of the stable isotopes, depending especially on the temperature conditions and the relative reaction rates [generally the (p, α) reactions are much faster than the (p, γ) reactions, hence ^{15}N, ^{18}O, ^{19}F, and ^{22}Ne disappear far more rapidly than the other stable isotopes during this early history].

In contrast, the character of the nuclear burning on long time scales is extremely temperature sensitive. At lower temperatures, $T_9 \leq 0.2$, once substantial abundances of ^{13}N, ^{14}O, and ^{15}O are achieved and the total burning time approaches or exceeds their decay lifetimes, the CNO bi-cycles characteristic of burning at lower temperatures (Caughlan and Fowler 1962) become evident. Since the $^{13}N(p, \gamma)^{14}O$ reaction is competitive with the $^{13}N(e^+\nu)^{13}C$ decay at these temperatures, the formation and decay of ^{14}O becomes a major distinguishing feature of these higher temperature cycles. This behavior is illustrated in figure 3, where the major flows for $T_9 = 0.1$, $\rho = 100$ g cm^{-3} at time $t \sim 10^5$ s are shown. The dominant sequence of reactions here is

$$^{12}C(p, \gamma)^{13}N(p, \gamma)^{14}O(e^+\nu)^{14}N(p, \gamma)^{15}O(e^+\nu)^{15}N(p, \alpha)^{12}C\,,$$

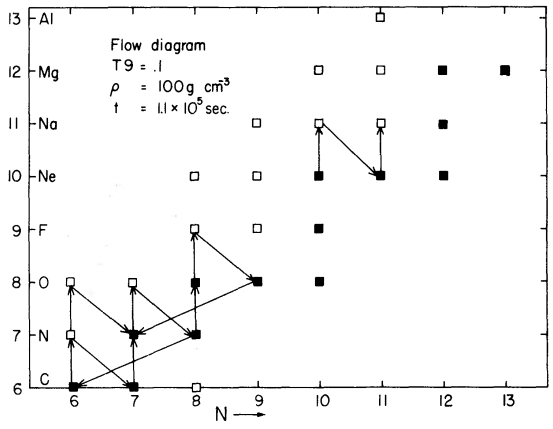

FIG. 3.—Flow diagram at $T_9 = 0.1$, $\rho = 100\ \mathrm{g\ cm^{-3}}$, and $t = 1.1 \times 10^5$ s. The standard CNO cycle is operating at these moderately high temperatures.

with weaker branches

$$^{13}\mathrm{N}(e^+\nu)^{13}\mathrm{C}(p,\gamma)^{14}\mathrm{N}$$

and

$$^{15}\mathrm{N}(p,\gamma)^{16}\mathrm{O}(p,\gamma)^{17}\mathrm{F}(e^+\nu)^{17}\mathrm{O}(p,\alpha)^{14}\mathrm{N}\,.$$

As long as the proton flux is not exhausted, we see here that one can get significant overabundances of masses 13, 14, 15, and 17 existing primarily as ^{13}N, ^{14}O, ^{15}O, and ^{17}F. These positron-emitting isotopes with characteristic lifetimes $\gtrsim 100$ s here play the same role as does ^{14}N at lower temperatures: their relatively slow rates of destruction dictate the time scales of these cycles and render them the most abundant constituents.

At higher temperatures, significant perturbations on these flow patterns become increasingly apparent. Figure 4 illustrates the major flows for $T_9 = 0.5$, $\rho = 100\ \mathrm{g\ cm^{-3}}$ at time $t = 10^5$ s. At this temperature the abundances of ^{14}O and ^{15}O become relatively large, as do the rates of α-induced reactions. Superposed upon the CNO cycling

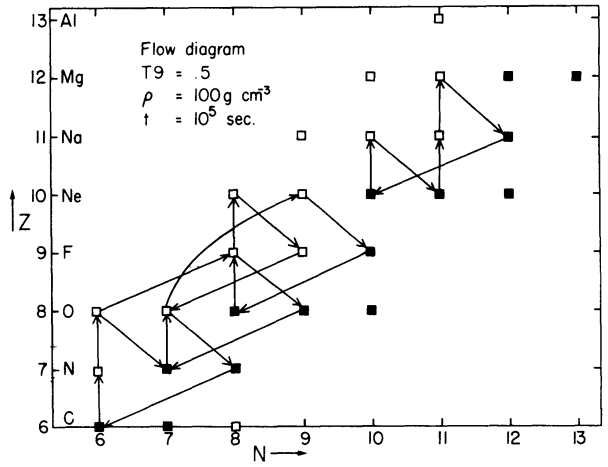

FIG. 4.—Flow diagram at $T_9 = 0.5$, $\rho = 100\ \mathrm{g\ cm^{-3}}$, $t = 10^5$ s. At this temperature the importance of $^{14}\mathrm{O}(\alpha, p)^{17}\mathrm{F}$, $^{15}\mathrm{O}(\alpha, \gamma)^{19}\mathrm{Ne}$, and $^{17}\mathrm{F}(p, \gamma)^{18}\mathrm{Ne}$ becomes apparent. Under these conditions the Ne-Na cycle also operates.

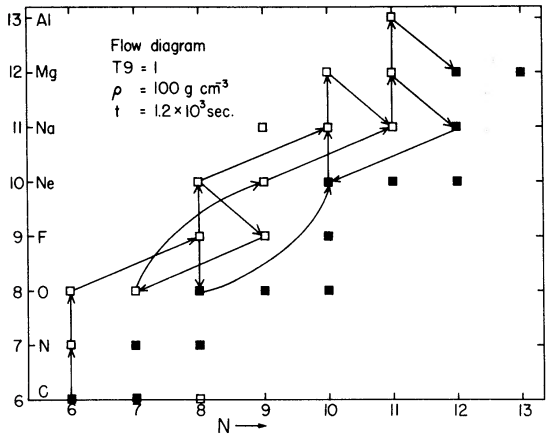

FIG. 5.—Flow diagram at $T_9 = 1$, $\rho = 100$ g cm^{-3}, and $t = 1.2 \times 10^3$ s. At this temperature the alpha-induced reactions transform the lighter elements C–F into the heavier ones up to ^{24}Mg.

patterns proceeding via ^{14}O, the contributions from the $^{14}O(\alpha, p)^{17}F$, $^{15}O(\alpha, \gamma)^{19}Ne$, and $^{17}F(p, \gamma)^{18}Ne$ reactions become important resulting in significant enhancements of masses 17, 18, and 19.

Furthermore, the neon-sodium (Ne-Na) cycle operating at these temperatures acts to enhance the abundances at masses 21 and 22:

$$^{20}Ne(p, \gamma)^{21}Na(e^+\nu)^{21}Ne(p, \gamma)^{22}Na\,,$$

$$^{22}Na(p, \gamma)^{23}Mg(e^+\nu)^{23}Na(p, \alpha)^{20}Ne\,.$$

These features are apparent at temperatures $T_9 = 0.5$ to 1.0 for densities $\rho \lesssim 100$ g cm^{-3}. At the highest temperatures and densities, $T_9 = 1$, $\rho \gtrsim 10^2$ g cm^{-3}, a rapid transformation of the lighter elements to the heavier nuclei takes place on rapid time scales (fig. 5) as a consequence of significant contributions from α-induced reactions: ^{15}O and ^{16}O go to ^{19}Ne and ^{20}Ne by (α, γ) reactions. The Ne-Na cycle continues to be important, assisting in the conversion of the bulk of the initial nuclei to ^{24}Mg following $^{23}Mg(p, \gamma)^{24}Al(e^+\nu)^{24}Mg$.

We now proceed to a discussion of the variations of abundances in time, keeping in mind the basic patterns of thermonuclear flows summarized in the previous paragraphs.

a) Evolution at $T_9 = 0.1$

The evolution of the mass fractions as a function of time are shown in figures 6*a* and 6*b* for a temperature $T_9 = 0.1$ and density $\rho = 100$ g cm^{-3}. The total abundances for a given mass are represented by the abundances of the stable nucleus at the mass number—equivalent to instantaneously turning off the temperature and allowing positron decays to proceed. At this density, the main enhancements achieved are those of ^{13}C (by a factor greater than 30), and ^{15}N and ^{17}O (by factors ~ 10) between 5×10^2 and 10^4 s. This results from relative enhancements of ^{13}N, ^{15}O, and ^{17}F. For these burning conditions, rather small enhancements are realized.

At the end of the nuclear processing we get ratios $^{15}N/^{14}N = 1.4 \times 10^{-2}$, $^{13}C/^{12}C = 1.3$, and N/C = 9.3, quite comparable with those obtained by Caughlan and Fowler (1972, 1973) but strongly different from those calculated in the "cold" CNO cycle (Caughlan and Fowler 1962) where the same ratios are, respectively, 4×10^{-5}, 0.3,

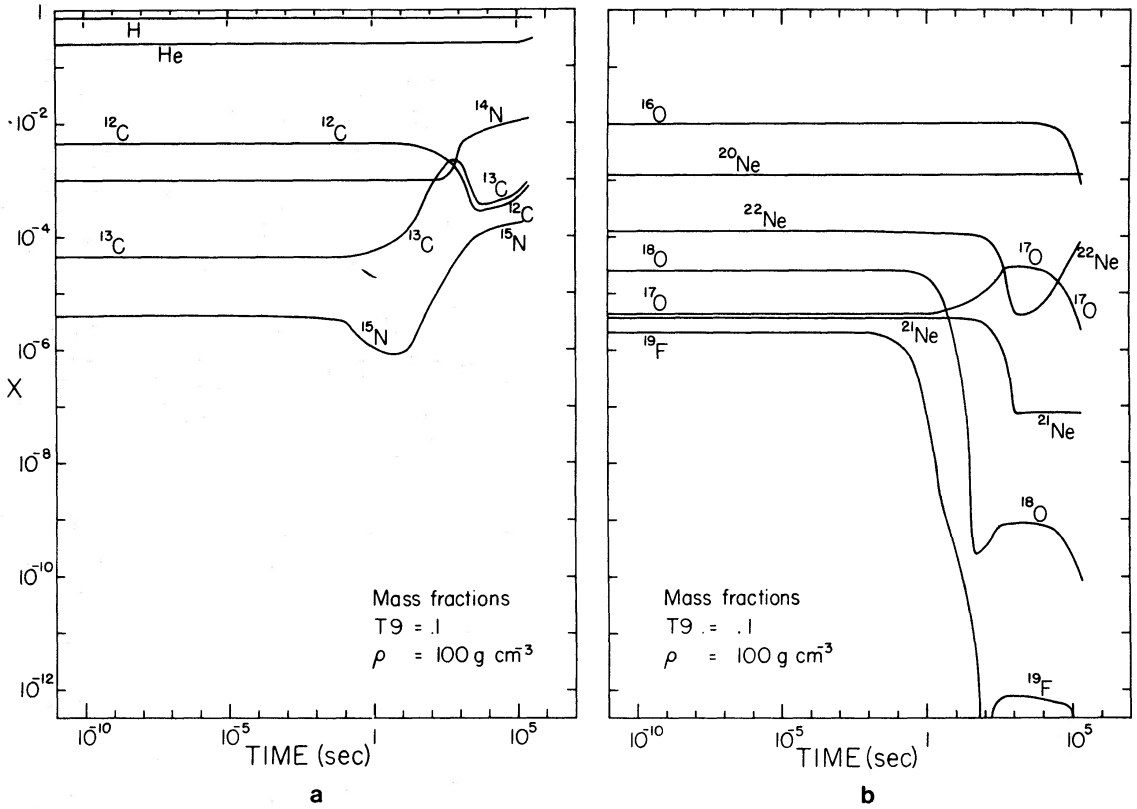

FIGS. 6*a* and 6*b*.—Evolution of the mass fractions X as a function of time for $T_9 = 0.1$ and $\rho = 100$ g cm^{-3}. ^{13}C, ^{14}N, and ^{15}N are slightly enhanced for $t \gtrsim 10^2$–10^3 s, while ^{18}O, ^{19}F, and ^{21}Ne are depleted.

and ~ 100. This illustrates the effects of the relative change in importance of the positron decay rates at these temperatures.

Table 2 summarizes the enhancements achieved as a function of density. Even for densities as high as 10^3 g cm^{-3} the effects are only interesting for ^{13}C and ^{15}N for time scales $\geq 10^2$–10^3 s. It must be noted, however, that such low temperatures are the most promising with regard to the production of ^{13}C, since ^{13}N is readily destroyed

TABLE 2

ENHANCEMENTS FOR $T_9 = 0.1$

ρ (g cm^{-3})	1		10		100		1000	
	x	t (s)	x	t (s)	x	t (s)	x	t (s)
H.....	...	...	...	...	...	...	~0.5	$>10^5$
He.....	...	...	...	...	...	...	~2	$>10^5$
^{13}C.....	~10	$>10^4$	~20	10^3–10^4	>30	10^2–2×10^3	~40	$>5 \times 10^2$
^{14}N.....	...	...	5	$>10^5$	10	$>10^5$	10	$\gtrsim 10^4$
^{15}N.....	0.1–0.3	>30	3	$>3 \times 10^4$	10–80	$>10^3$	20–300	10^2–10^4
^{17}O.....	3	~10^5	2	3×10^3	7	5×10^2–2×10^4	>10	10–10^4

NOTE.—The enhancement (or sometimes depletion) factors x [$X(A)_{\text{calculated}}/X(A)_{\text{solar system}}$] are gathered for different densities together with the time scale t (in seconds) where these enhancements (or depletions) are obtained.

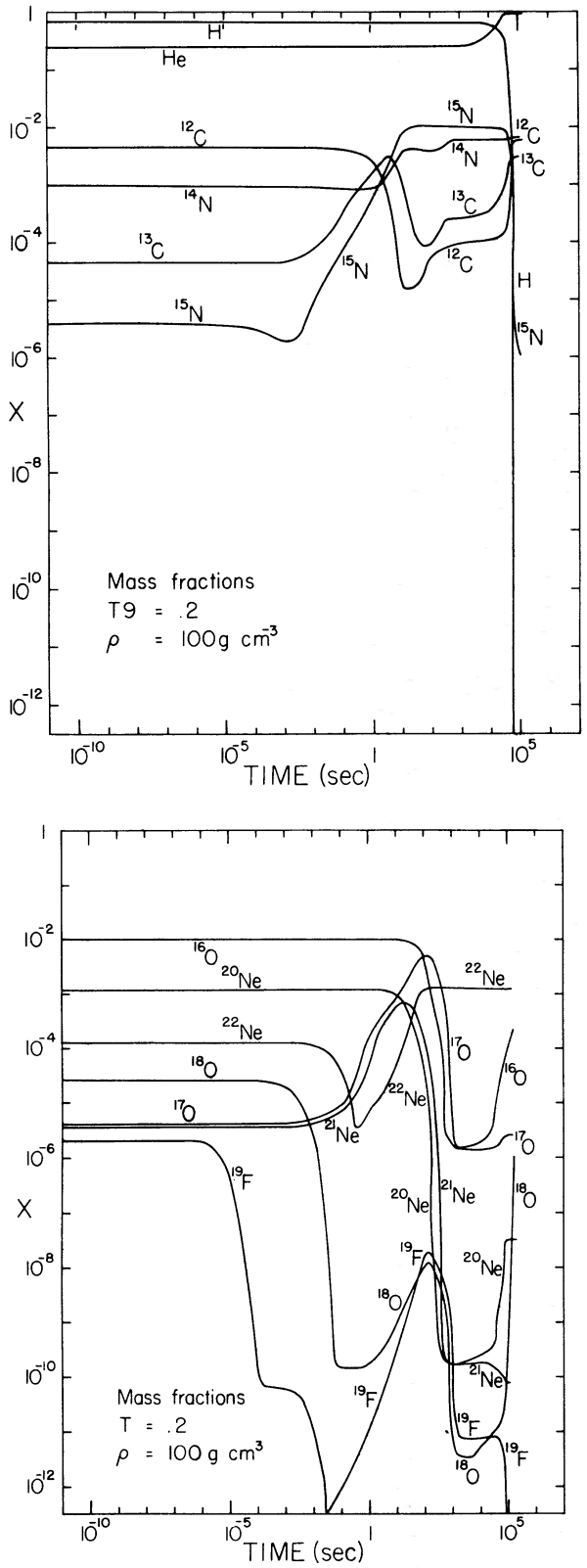

FIGS. 7*a* (*top*) and 7*b* (*bottom*).—Evolution of the mass fractions X as a function of time for $T_9 = 0.2$ and $\rho = 100$ g cm^{-3}. Notice the transformation of hydrogen into helium at $t \sim 3 \times 10^4$ s and the enhancements in ^{13}C, ^{14}N, ^{15}N, ^{17}O, and ^{21}Ne. ^{18}O and ^{19}F are still depleted at such temperatures.

TABLE 3

ENHANCEMENTS FOR $T_9 = 0.2$

ρ (g cm^{-3})	1		10		100		1000	
	x	t (s)	x	t (s)	x	t (s)	x	t (s)
H → He* . . .	. . .	. . .	H → He	3×10^4	H → He	3×10^4	H → He	3×10^4
^{13}C	> 50	> 100	> 20	> 3	10–60	0.03–10	10–50	0.03–1
^{14}N	~ 2	10^4	5	10^4	5	3×10^3	5	$\sim 10^3$
^{15}N	10^2–5×10^2	10^2–10^4	10^2–2×10^3	10–10^4	10^2–2×10^3	1–5×10^4	10^2–2.5×10^3	0.03–5×10^4
^{17}O	30–200	10^2–10^4	30–300	10–3×10^3	10^2–10^3	3–600	10^2–2×10^3	0.3–300
^{21}Ne	~ 5	10^2–10^3	10–100	10–500	30–150	2–100	30–200	0.2–100
^{22}Ne	> 10	~ 10^4	> 10	~ 10^3	> 10	~ 10^2	> 10	~ 10^2

* Time necessary to transform all H into He.

NOTE.—The enhancement (or sometimes depletion) factors x [$X(A)_{\text{calculated}}/X(A)_{\text{solar system}}$] are gathered for different densities together with the time scale t (in seconds) where these enhancements (or depletions) are obtained.

by the $^{13}N(p, \gamma)^{14}O$ reaction at higher temperatures. This important feature will be discussed in greater detail in the following section.

b) *Evolution at* $T_9 = 0.2$

The variations in the elemental fractions with time at a temperature $T_9 = 0.2$ and density $\rho = 100$ g cm^{-3} (figs. 7*a* and 7*b*) are qualitatively the same as for the $T_9 = 0.1$ case. The enhancements realized as a function of density are shown in table 3. The main features may be summarized briefly as follows.

Hydrogen is completely transformed into helium at about 3×10^4 s, this time being independent of the density (see table 3). This behavior is illustrative of the fact that the time scale of the hot CNO cycle is largely governed by the β-decay rates, rather independent of density and temperature. Overabundances of ^{13}C, ^{15}N, ^{17}O, ^{21}Ne, and ^{22}Ne are realized at various stages of burning: ^{13}C by a factor $\gtrsim 10$, ^{15}N by factors as large as 2000 for times $10 \leq t \leq 10^4$ s, ^{17}O by a factor $\gtrsim 100$ over the time interval from ~ 3 to 600 s, ^{21}Ne by a factor $\gtrsim 30$ for burning times between ~ 2 and 100 s, and ^{22}Ne by a factor $\gtrsim 10$ for times $t \gtrsim 10$ s.

Two features of these abundance histories deserve further comment. We note first that for times $t > 1$ s, prior to hydrogen exhaustion, the $^{13}C/^{12}C$ ratio exceeds unity, far out of line with the steady-state ratio $^{13}C/^{12}C = 0.3$ characteristic of burning at temperatures below 10^{8} ° K. This results from the fact that the major destruction of mass 13 here takes place by the $^{13}N(p, \gamma)^{14}O$ reaction. The ratio can now approach a steady-state value $^{13}C/^{12}C \sim \tau[^{13}N(p, \gamma)^{14}O]/\tau[^{12}C(p, \gamma)^{13}N]$ which itself exceeds one. The late rise in the ^{12}C and ^{13}C abundances and the associated inversion of the ratio to $^{12}C/^{13}C > 1$ results from the $^{15}N(p, \alpha)^{12}C$ reaction which proceeds rapidly following the $^{15}O(e^{+}\nu)^{15}N$ decay.

The peaking and subsequent fall-off of the abundances of masses 17, 18, 19, and 21 are persistent features of burning at high temperatures which have strong implications for nucleosynthesis. The abundances at these mass numbers increase rapidly over burning intervals $\sim$1–100 s, primarily due to (p, γ) reactions. On longer time scales, the positron decays of the positron-unstable isotopes ^{17}F, ^{18}Ne, ^{19}Ne, and ^{21}Na (lifetimes of 66, 1.5, 17.5, and 22.8 s, respectively) begin to dominate, and the abundances at these mass numbers fall toward their much lower steady-state values, defined by equality of the rates of formation and destruction. The production of enhanced abundances of nuclei at these mass numbers (^{17}O, ^{18}O, ^{19}F, and ^{21}Ne) must therefore require burning time scales in real astrophysical environments which do not greatly exceed the decay lifetimes of the unstable progenitors of these isotopes.

c) *Evolution at* $T_9 = 0.5$

The abundance histories for burning at $T_9 = 0.5$ are shown for a density $\rho = 100$ g cm^{-3} in figures 8*a* and 8*b*, and for a density $\rho = 1000$ g cm^{-3} in figures 9*a* and 9*b*. The enhancements realized as a function of density are shown in table 4. Burning at this higher temperature differs in several important respects from the previous cases. The $^{13}C/^{12}C$ ratio is again greater than unity, but the abundances at both mass numbers have been enormously depleted as a significant fraction of the material is processed toward higher masses. Significant ^{13}C production clearly can take place only at lower temperatures.

Large enhancements of masses 15, 17, and 21 (^{15}N, ^{17}O, and ^{21}Ne) and lesser maximum overabundances at masses 18, 19, and 22 (^{18}O, ^{19}F, and ^{22}Ne) are evident at various phases of the burning histories. Following the fall-off from their peak values achieved at times $t \lesssim \tau_{e^+}$, the abundances of ^{18}O, ^{19}F, and ^{21}Ne tend to fall off rapidly at long times ($t \gtrsim 10^4$ s) due to the combined effects of positron decay of ^{18}Ne, ^{19}Ne, and ^{21}Na and (p, α) reactions near hydrogen exhaustion. At higher

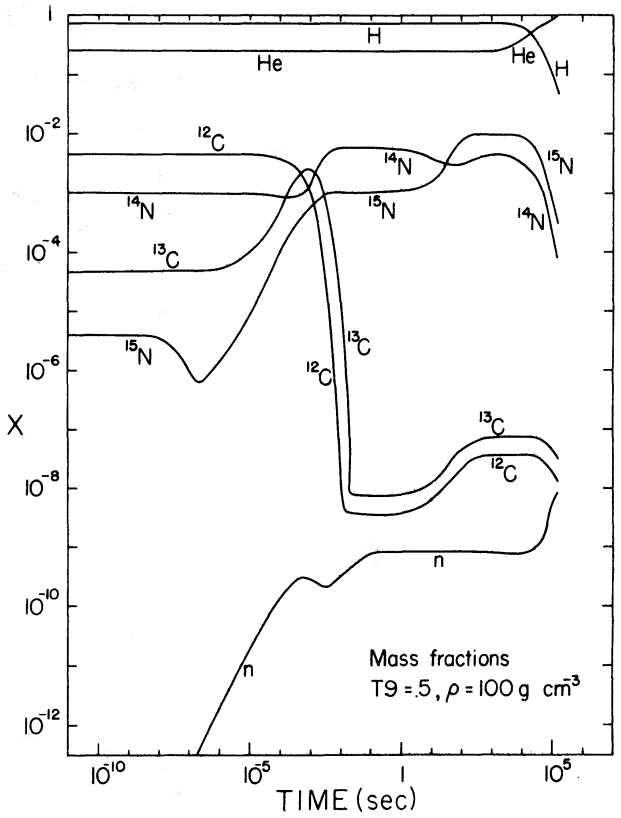

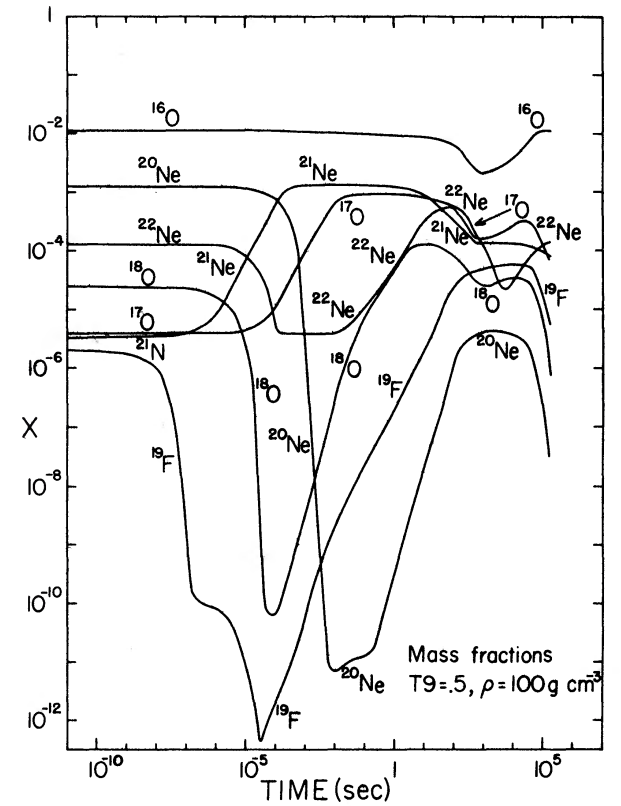

FIGS. 8*a* (*top*) and 8*b* (*bottom*).—Evolution of the mass fractions X as a function of time for $T_9 = 0.5$ and $\rho = 100$ g cm^{-3}. Notice the enhancement of ^{15}N and the production of $\sim 10^{-9}$ neutrons (by mass), while ^{12}C and ^{13}C are depleted after times as short as 10^{-3} s. At this temperature ^{18}O and ^{19}F begin to be formed.

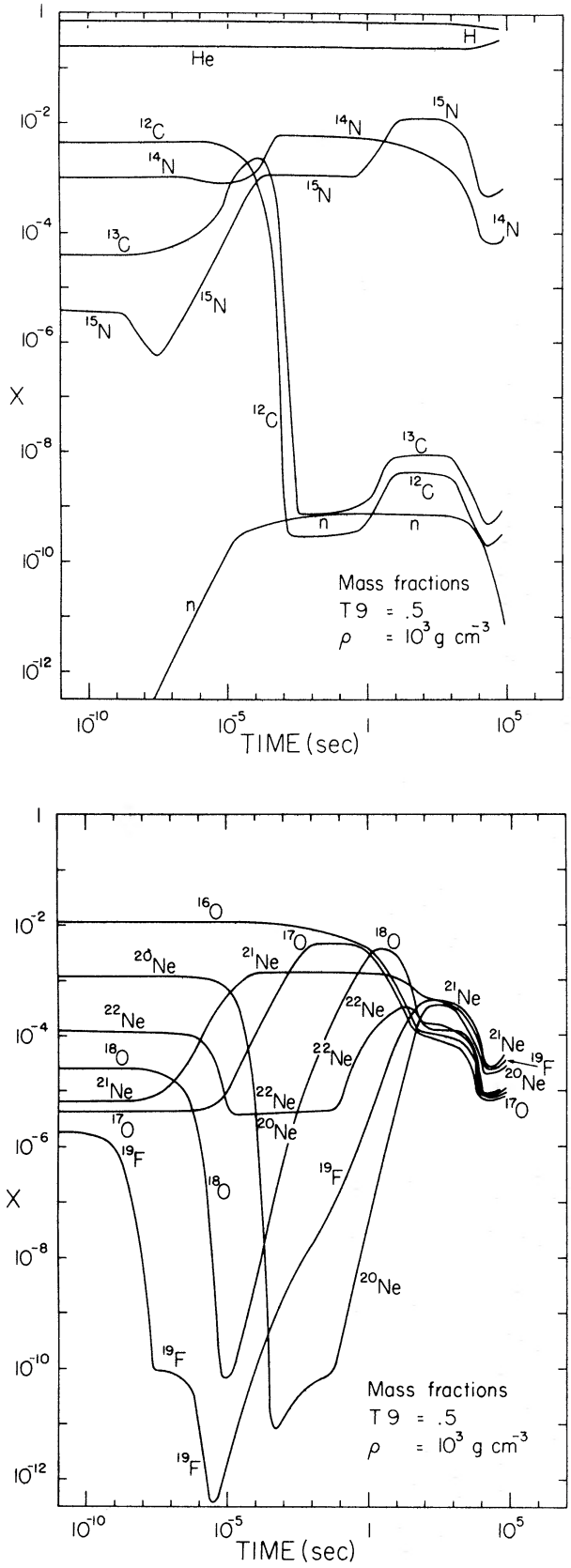

FIGS. 9*a* (*top*) and 9*b* (*bottom*).—Evolution of the mass fractions X as a function of time for $T_9 = 0.5$ and $\rho = 10^3$ g cm^{-3}. At such temperature and density conditions the (α, p) reactions prevent the transformation of hydrogen into helium.

TABLE 4

ENHANCEMENTS FOR $T_9 = 0.5$

ρ	1		10		100		10^3	
(g cm^{-3})	x	t (s)	x	t (s)	x	t (s)	x	t (s)
H $\rightarrow$ He*...	...	3×10^4–10^5	...	3×10^4	...	3×10^4	...	$\gtrsim 10^5$
$X(n)$†.....	10^{-9}–10^{-7}	$>10^3$	$>7 \times 10^{-10}$	>1	$>8 \times 10^{-10}$	>0.1	$>3 \times 10^{-10}$	$>3 \times 10^{-5}$
^{13}C.....	>10	6×10^{-3}–5×10^{-1}	>10	5×10^{-4}–5×10^{-2}	>10	5×10^{-5}–5×10^{-3}	>10	10^{-3}–6×10^{-4}
^{14}N.....	5	1–10	5	5×10^{-2}–3	5	5×10^{-3}–1	5	5×10^{-4}–1
^{15}N.....	100–10^3	$>5 \times 10^{-2}$	100–10^3	$>5 \times 10^{-3}$	100–2.6×10^3	5×10^{-4}	100–3100	$>4 \times 10^{-5}$
^{17}O.....	2	$>10^{-2}$	10–20	$>5 \times 10^{-3}$	30–200	$>2 \times 10^{-3}$	30–1200	2×10^{-4}–10^{-2}
^{18}O.....	5×10^{-4}	10–10^4	5×10^{-2}	0.3–3×10^3	2–5	1–200	10–120	10^{-1}–50
^{19}F.....	>0.1	10^3–10^5	>1	3×10^2–10^5	10–25	>50	10–200	>5
^{21}Ne.....	30–330	1.5×10^{-3}–80	30–400	10^{-4}–160	30–330	10^{-5}–10^5	30–500	10^{-6}–5×10^3
^{22}Ne.....	10	30–6×10^3	10	50–600	2–4.5	5–500	>2	5–50

* Time necessary to transform all H into He.

† Mass fraction $X(n)$ of neutrons with respect to the time.

NOTE.—The enhancement (or sometimes depletion) factors x [$X(A)_{\text{calculated}}/X(A)_{\text{solar system}}$] are gathered for different densities together with the time scale t (in seconds) where these enhancements (or depletions) are obtained.

densities (figs. 9*a* and 9*b*), the effects of (α, p) reactions are to somewhat slow down the rate of hydrogen depletion; after 10^5 s the hydrogen abundance has fallen only slightly while small overabundances at masses 17, 18, 19, and 21 are still evident.

The production of a neutron abundance $\sim 10^{-9}$ by mass is also seen to occur at this temperature for times up to $\sim 10^5$ s. This results primarily from (α, n) reactions proceeding on ^{13}C, ^{17}O, ^{18}O, ^{21}Ne, and ^{22}Ne. As the ^4He abundance increases in the late stages of burning (figs. 8*a* and 9*a*), the neutron abundance also increases. The maximum neutron concentrations realized at this temperature are not sufficient to drive a full *s*-process, but they may result in modifications of the abundances of iron-peak nuclei present in the same material.

d) *Evolution at* $T_9 = 1.0$

The variations of the mass fractions with time resulting from burning at a temperature of one billion degrees are shown for densities $\rho = 100$ and 1000 g cm^{-3} in figures 10*a*, 10*b*, 11*a*, and 11*b*. Table 5 summarizes the overabundances of various mass numbers as a function of density. At this high temperature, a combination of (α, p) and (γ, p) reactions act to retard the rate of hydrogen depletion. Neutron concentrations approaching $\sim 10^{-7}$ by mass are realized here for times up to ~ 1000 s; again no significant neutron processing of nuclei above iron can result from this neutron flux.

As in the previous case, large overabundances of many of the more massive nuclei—

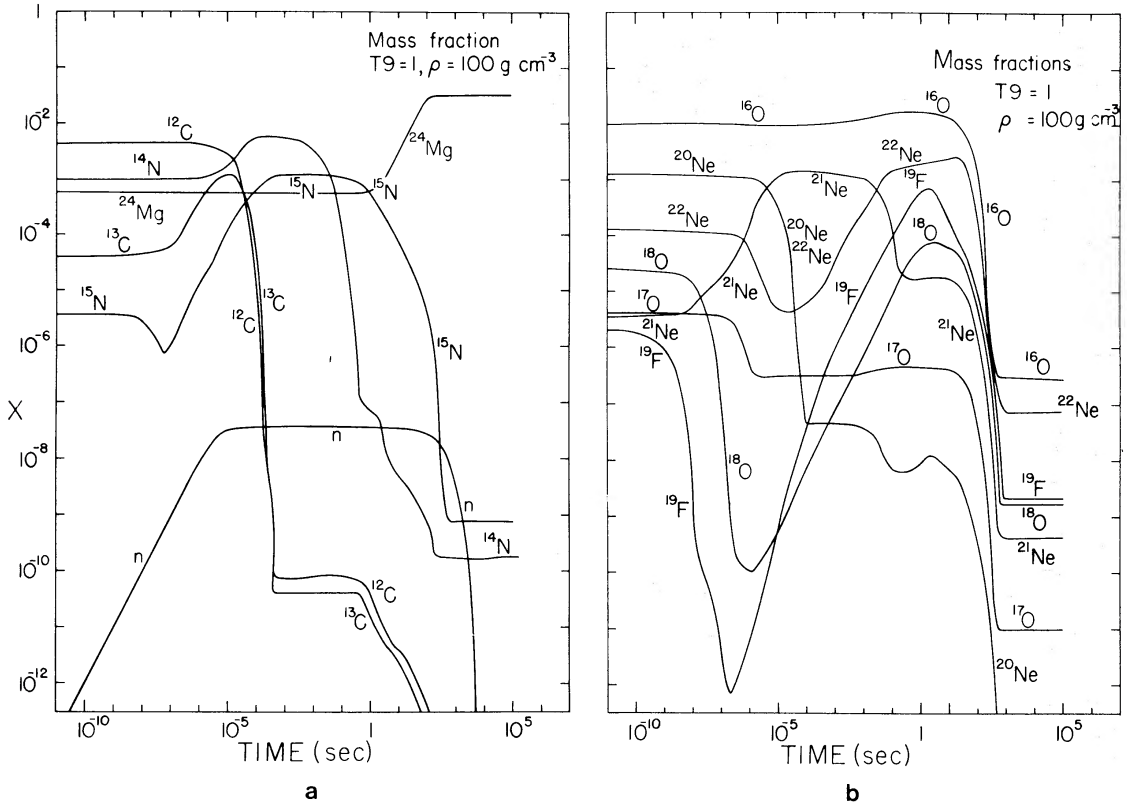

FIGS. 10*a* and 10*b*.—Evolution of the mass fractions X as a function of time for $T_9 = 1$ and $\rho = 100$ g cm^{-3}. Notice the increase of $X(^{24}Mg)$ due to the transformation of the lighter nuclei by α-particle induced reactions. The hydrogen and helium mass fractions (not illustrated) remain constant throughout the duration of the process.

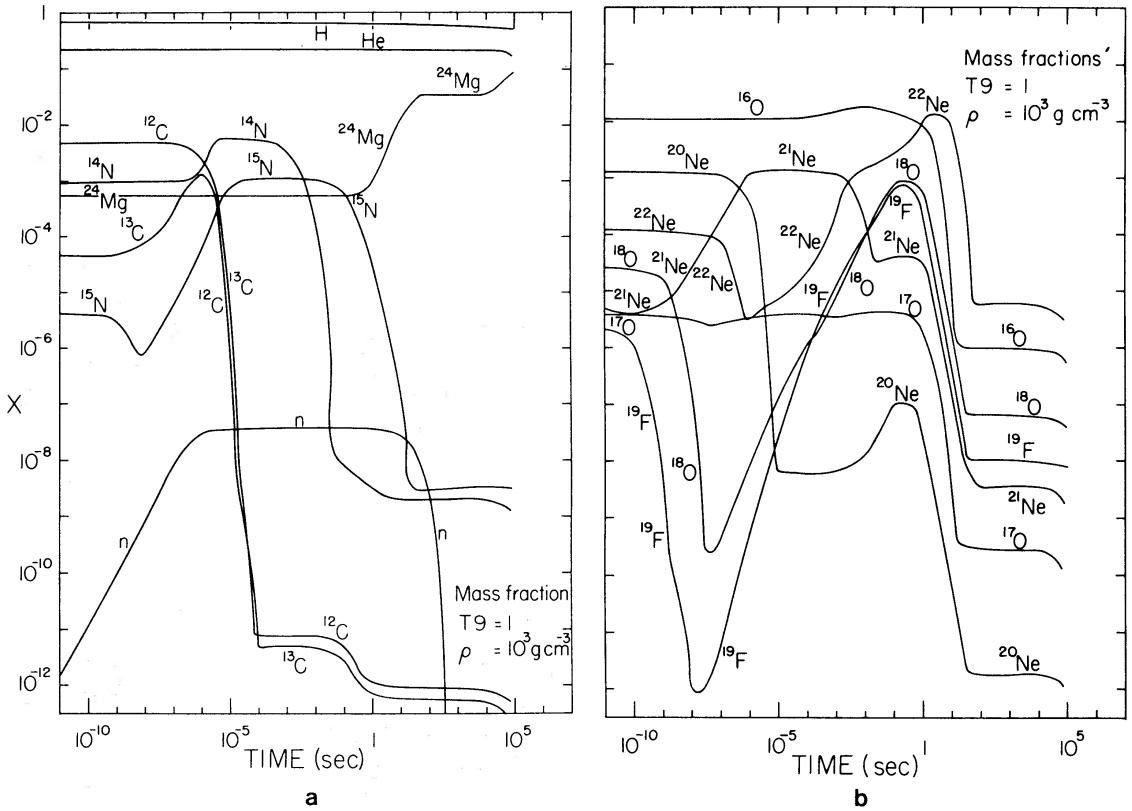

FIGS. 11*a* and 11*b*.—Evolution of the mass fractions X as a function of time for $T_9 = 1$ and $\rho = 10^3$ g cm^{-3}.

^{18}O, ^{19}F, ^{21}Ne, and ^{22}Ne—together with ^{15}N occur at various times relatively early in the burning. Oxygen-17 is not enhanced at this temperature. This is due to the fact that the rate of ^{17}F$(\gamma, p)^{16}$O overcomes that of ^{16}O$(p, \gamma)^{17}$F, and ^{13}C is again greatly depleted. The interesting new feature is that if the burning is allowed to proceed for a time in excess of $\gtrsim 100$ s, no enhancement of any of these rarer isotopes is achieved. The net result of such burning is the transformation of the major fraction of the mass initially present in the form of nuclei heavier than ^{4}He to ^{24}Mg—the burning has simply gone too far. If the burning could somehow be instantaneously terminated at a time ~ 10 s, the net result would be large enhancements of nuclei of mass 15, 18, 19, 21, and 22. In the following section we will discuss qualitatively the likelihood of such behavior in the context of hydrodynamic expansion and cooling of mass zones ejected in nova and supernova explosions.

IV. NUCLEOSYNTHESIS IN HIGH-TEMPERATURE HYDROGEN BURNING

The presentation of the results of our calculations in the previous section has involved some attention to detail, intended for those concerned with the specific characteristics of this thermonuclear burning process. This study of nuclear "cooking" at constant density and temperature will be useful in subsequent studies where detailed variations of density and temperature with respect to time (representing, for instance, the ejecta of novae, supernovae, or supermassive star explosions) must be considered. For instance, the preliminary results obtained by Audouze and Fricke (1973) in their study of hydrogen burning in supermassive star explosions are very similar to those obtained here for $T_9 = 0.2$ and predictions of nucleosynthesis in nova envelopes

TABLE 5

ENHANCEMENTS FOR $T_9 = 1$

ρ ($g\,cm^{-3}$)	1		10		100		1000	
	x	t (s)	x	t (s)	x	t (s)	x	t (s)
$X(n)$*	10^{-8}–3.5×10^{-8}	10^{-4}–4×10^{4}	10^{-8}–3.5×10^{-8}	2×10^{-5}–3×10^{3}	10^{-8}–3.5×10^{-8}	10^{-6}–400	10^{-8}–3.5×10^{-8}	10^{-7}–40
^{13}C...	10–17	2×10^{-4}–4×10^{-3}	10–25	2×10^{-5}–3×10^{-4}	10–25	10^{-6}–4×10^{-5}	10–25	2×10^{-7}–3×10^{-6}
^{14}N...	5	5×10^{-2}–2×10^{-1}	5	5×10^{-4}–3×10^{-2}	5	10^{-4}–10^{-3}	5	3×10^{-6}–3×10^{-4}
^{15}N...	100–300	4×10^{-3}–80	100–300	3×10^{-4}–8	100–300	4×10^{-5}–2	100–300	3×10^{-6}–0.4
^{17}O...	10^{-3}	3×10^{-4}–2×10^{-3}	10^{-2}	3×10^{-5}–300	~ 0.1	2×10^{-6}–20	< 1	> 10
^{18}O...	10^{-3}	10–500	0.1	3–100	2–3	0.5–20	10–36	3×10^{-2}–3
^{19}F...	10–60	2–200	10–200	0.9–100	10–300	2×10^{-2}–60	10–350	2×10^{-3}–20
^{21}Ne..	30–400	4×10^{-3}–600	30–400	8×10^{-6}–1.2	30–400	8×10^{-7}–10^{-1}	30–400	5×10^{-8}–10^{-2}
^{22}Ne..	2–5	0.5–10^{3}	2–10	0.1–300	2–20	10^{-2}–100	10–100	5×10^{-3}–20

* Mass fraction $X(n)$ of neutrons with respect to the time.

NOTE.—The enhancement (or sometimes depletion) factors x [$X(A)_{\text{calculated}}/X(A)_{\text{solar system}}$] are gathered for different densities together with the time scale t (in seconds) where these enhancements (or depletions) are obtained.

(Starrfield *et al.* 1972, 1973) are grossly compatible with our results for the nuclear evolution at $T_9 = 0.5$. The significant consequences of high-temperature CNO–Ne cycle burning for nucleosynthesis as inferred from our studies are summarized below.

a) The transformation of hydrogen to helium takes place on a time scale which is not a simple function of the burning temperature and density. The time scale for hydrogen exhaustion decreases from $\sim 10^7$ s at $T_9 = 0.1$ to $\sim 10^5$ s for $T_9 = 0.2$, primarily as a result of the temperature sensitivity of the proton capture reaction rates. At $T_9 = 0.5$, competition from (γ, p) reactions reduced the effectiveness of increased (p, γ) reactions and the burning time scale remains at $\sim 10^5$ s. At the highest temperature studied, $T_9 = 1$, both (γ, p) and (α, p) reactions act strongly to oppose hydrogen exhaustion. Furthermore, the buildup proceeds toward heavier nuclei, $A \gtrsim 19$, where the importance of reaction cycles in the conversion of hydrogen to helium is reduced. At this temperature, the time scale for hydrogen exhaustion increases to $\sim 10^6$ s, somewhat dependent upon the density.

b) A small neutron flux can be achieved at higher temperatures for times of the order of ~ 1000 s. We found, specifically, a neutron mass fraction greater than 10^{-9} maintained for $\sim 10^5$ s in burning at $T_9 = 0.5$, and a neutron mass fraction greater than $\sim 10^{-8}$ maintained for more than $\sim 10^3$ s at $T_9 = 1.0$. These neutrons result primarily from (α, n) reactions which can proceed rapidly at higher burning temperatures. The $^{14}\mathrm{N}(n, p)^{14}\mathrm{C}$ reaction acts to moderate the neutron fluxes at these levels. These neutron concentrations clearly are not sufficient to drive a full *s*-process: the ratio of neutrons to seed ^{56}Fe nuclei (for solar material) is only $10^{-8}/2 \times 10^{-5} \sim 5 \times 10^{-4}$, while a ratio ~ 10–100 is required for significant buildup by neutron capture.

c) The production of ^{13}C is strongly temperature dependent. Significant overproduction of ^{13}C occurs only at lower temperatures, $T_9 \lesssim 0.2$. At higher temperatures, even though the $^{13}\mathrm{C}/^{12}\mathrm{C}$ ratio typically exceeds unity, the total abundances of both carbon isotopes are reduced by several orders of magnitude relative to solar proportions, primarily due to the reaction sequence $^{12}\mathrm{C}(p, \gamma)^{13}\mathrm{N}(p, \gamma)^{14}\mathrm{O}$. The large ^{13}C abundances observed in carbon stars, $^{12}\mathrm{C}/^{13}\mathrm{C} \sim 0.3$, C/O > 1, presumably result from CNO-cycle burning at temperatures below 200 million degrees (Scalo and Ulrich 1973; Sackmann, Smith, and Despain 1973; Truran 1973).

d) The isotopes of nitrogen, ^{14}N and ^{15}N, are both enhanced, particularly at lower temperatures, due to the relative stability of their positron-decay progenitors, ^{14}O and ^{15}O, against proton-induced reactions. The enhancement of ^{14}N never exceeds a factor ~ 6 in the temperature range explored in this paper, supporting indirectly the usual view that ^{14}N results from CNO-cycle hydrogen burning at lower temperatures. Nitrogen-15, in contrast, is the most readily overproduced isotope for the burning conditions explored in this paper. Significant enhancements occur, particularly at temperatures above $T_9 = 0.2$, with some reduction at mass $A = 15$ resulting at a temperature $T_9 = 1.0$ due to the increased importance of the $^{15}\mathrm{O}(\alpha, \gamma)^{19}\mathrm{Ne}$ reaction forming mass $A = 19$.

e) Of the rare isotopes of oxygen, ^{17}O is readily enhanced for temperatures below $T_9 \sim 0.5$ and larger densities ($\rho \gtrsim 100$ g cm^{-3}). At higher temperatures and lower densities competition from the $^{17}\mathrm{F}(\gamma, p)^{16}\mathrm{O}$ reaction seriously inhibits the production at mass $A = 17$.

Any initial ^{18}O present in the medium is readily destroyed even at lower temperatures, $T_9 \lesssim 0.2$, by the reaction $^{18}\mathrm{O}(p, \alpha)^{15}\mathrm{N}$. Even under circumstances where mass $A = 18$ is formed as ^{18}F, this will in turn be destroyed by $^{18}\mathrm{F}(p, \gamma)^{19}\mathrm{Ne}$. A significant enhancement at mass $A = 18$ occurs only at intermediate temperatures $T_9 \sim 0.5$ and densities $\rho \gtrsim 100$ g cm^{-3} by means of the $^{17}\mathrm{F}(p, \gamma)^{18}\mathrm{Ne}$ reaction. Even under these more favorable conditions, mass $A = 18$ is destroyed if the burning proceeds on time scales long enough for the weak interactions to take place. Following ^{18}Ne decay,

$^{18}F(p, \alpha)^{15}O$ proceeds rapidly and any $^{18}F(e^+\nu)^{18}O$ decay is immediately followed by $^{18}O(p, \alpha)^{15}N$.

f) Large overabundances of ^{19}F are found to occur only for CNO–Ne cycle burning at higher temperatures and densities. Under these circumstances, mass $A = 19$ is produced as ^{19}Ne by the $^{15}O(\alpha, \gamma)^{19}Ne$ and, to a lesser extent, the $^{18}F(p, \gamma)^{19}Ne$ reactions. Enhancements of factors $\gtrsim 100$ can be achieved for temperatures $T_9 \gtrsim 0.5$ and densities $\rho \gtrsim 100$ g cm^{-3}. The burning time scale is again a critical factor, for if the $^{19}Ne(e^+\nu)^{19}F$ decay takes place while the medium is still hot ($T_9 \gtrsim 0.2$), the ^{19}F thus formed will be rapidly destroyed by the $^{19}F(p, \alpha)^{16}O$ reaction.

g) The rare isotopes of neon are both produced in varying amounts in burning at higher temperatures. Overabundances of ^{22}Ne result from burning at temperatures $T_9 \gtrsim 1$ and densities $\rho \gtrsim 100$ g cm^{-3}. Under these conditions, significant production of mass $A = 22$ occurs by $^{21}Na(p, \gamma)^{22}Mg$. Following decay, $^{22}Mg(e^+\nu)^{22}Na$, the long-lived ^{22}Na can survive at somewhat higher temperatures than the progenitors of other rare isotopes.

Large overabundances of mass $A = 21$, reaching factors ~ 400, can also result for temperatures $T_9 \gtrsim 0.5$ as a result of the $^{20}Ne(p, \gamma)^{21}Na$ reaction. The disadvantage here again lies in the fact that ^{21}Na is relatively short lived and, following $^{21}Na(e^+\nu)^{21}Ne$, can be rapidly destroyed by $^{21}Ne(p, \alpha)^{18}F$ and $^{21}Ne(p, \gamma)^{22}Na$.

h) The triple-α reaction has been included in our reaction network. Its rate at temperature $T_9 < 1$ is too slow to induce significant transformation of ^4He into metals on the time scales we have considered in this paper. However, at $T_9 = 1$ some buildup of heavier nuclei by means of this reaction is realized. The strong increase in the ^{24}Mg concentration at long times ($t > 10^4$ s) evidenced in figure 11*a*, for instance, may be directly attributed to the inclusion of this reaction.

We see than that the rare isotopes of lighter nuclei—^{13}C, ^{15}N, ^{17}O, ^{18}O, ^{19}F, ^{21}Ne, and ^{22}Ne—can all be produced in enhanced concentrations under conditions where hydrogen burning proceeds via CNO–Ne cycles at higher temperatures. The precise conditions of maximum enhancement of these various isotopes vary considerably as a function of temperature, density, and burning time scale. The main features of these variations are summarized in table 6, where we have presented the ratios of our calculated abundances to the solar-system abundances (Cameron 1968) as a function of temperature, density, and burning time. The chosen burning times, $t = 5$, 50, and 500 s, correspond roughly to the hydrodynamic time scale given by Fowler and Hoyle (1964)

$$\tau_{HD} \sim 446/\rho^{1/2} \text{ seconds}$$

for densities $\rho = 10^4$, 10^2, and 1 g cm^{-3}, respectively. This is consistent with the view that such high-temperature hydrogen-burning conditions would most likely be achieved as a consequence of stellar explosions—novae or supernovae. For purposes of comparison, in constructing table 7 we have selected, for $T_9 = 0.5$ and 1.0 and densities $\rho = 1$, 10, 10^2, and 10^3 g cm^{-3}, the time scale for which the greatest number of nuclear species is enhanced. This table again gives the ratio of calculated to observed abundances.

These tables clearly illustrate the very complex character of the thermonuclear burning sequences explored in this paper. Abundances may be enhanced or depleted significantly depending on relatively small variations in any of the physical conditions considered—temperature, density, or time scale. We note as well that these calculations have been performed at constant temperature and density—we expect that the influence of expansion and cooling ("freezing") on the thermonuclear evolution of mass zones ejected in stellar explosions may alter the abundance patterns. The need for such freezing effects—for example, the need to reduce the temperature on a rapid time scale in order to preserve concentrations at masses $A = 18$, 19, and 21—is suggested by these constant-temperature studies.

TABLE 6

DEPLETIONS AND ENHANCEMENTS RELATIVE TO THE SOLAR ABUNDANCES FOR VARIOUS (T_9) CONDITIONS AND SPECIFIC TIME SCALES (5, 50, 500 seconds)

ELEMENT	SOLAR ABUNDANCES	TIME (s)	$T_9 = 0.1$		$T_9 = 0.2$		$T_9 = 0.5$		$T_9 = 1$	
			$\rho = 1$ g cm^{-3}	$\rho = 100$ g cm^{-3}	$\rho = 1$ g cm^{-3}	$\rho = 100$ g cm^{-3}	$\rho = 1$ g cm^{-3}	$\rho = 100$ g cm^{-3}	$\rho = 1$ g cm^{-3}	$\rho = 100$ g cm^{-3}
^{13}C.....	4.6×10^{-5}	5	1.0	1.9	3.0	50	2.0(−2)	2.2(−4)	1.1(−3)	8.1(−8)
		50	1.1	9.3	24	1.8	4.4(−2)	7.8(−4)	5.7(−5)	1.2(−8)
		500	1.8	44	520	5.9	6.5(−2)	1.5(−3)	4.3(−7)	1.2(−9)
^{14}N.....	9.7×10^{-4}	5	1.0	1.0	1.0	2.4	5.0	5.0	0.90	1.3(−5)
		50	1.0	1.0	1.0	3.8	3.6	3.5	0.01	1.9(−5)
		500	1.0	1.5	1.5	5.6	2.3	4.2	8.0(−5)	1.9(−7)
^{15}N.....	3.8×10^{-5}	5	0.90	0.23	4.8	270	350	400	300	23
		50	0.20	1.1	64	930	770	1400	170	3.1
		500	0.23	8.7	290	2700	1100	2600	1.5	2.4(−4)
^{17}O.....	4.3×10^{-6}	5	1.0	1.1	2.3	140	2.0	190	1.0(−3)	0.095
		50	1.0	2.1	15	930	2.0	150	1.1(−3)	0.028
		500	1.1	5.2	110	100	2.0	44	9.0(−4)	2.2(−6)
^{18}O.....	2.5×10^{-5}	5	1.0	0.3	2.0(−5)	2.4(−5)	4.8(−4)	4.6	6.5(−4)	2.8
		50	0.9	1.0(−5)	5.0(−3)	3.6(−4)	6.0(−4)	4.2	9.4(−4)	0.84
		500	0.44	3.0(−5)	0.16	4.0(−5)	5.7(−4)	1.2	9.0(−4)	6.4(−5)
^{19}F.....	2.0×10^{-6}	5	0.85	7.0(−4)	5.0(−7)	5.5(−5)	5.0(−3)	0.63	23	220
		50	0.27	3.0(−8)	1.9(−4)	5.0(−3)	4.6(−2)	7.9	75	16
		500	1.1(−3)	4.0(−7)	3.3(−2)	1.0(−3)	0.09	21	0.8	1.0(−3)
^{21}Ne.....	3.6×10^{-6}	5	1.0	1.0	1.2	70	330	330	110	5.2
		50	1.0	0.83	4.3	140	75	120	48	1.7
		500	1.0	2.3(−2)	4.7	2.5(−3)	2.4	39	31	1.2(−4)
^{22}Ne.....	1.3×10^{-4}	5	1.0	0.95	1.0	0.22	3.4	1.7	4.9	19
		50	1.0	0.78	1.1	6.5	9.2	5.6	2.2	8.5
		500	1.0	0.22	2.8	11	11	1.8	1.5	5.2(−4)

TABLE 7

SELECTION OF A FEW TEMPERATURE–DENSITY–TIME-SCALE CONDITIONS WHERE A LARGE NUMBER OF SIMILAR ENHANCEMENTS $x(A)$ ARE OBTAINED
$[x(A) = X(A)_{\text{calculated}}/X(A)_{\text{solar abundance}}]$

	$T_9 = 0.5$				$T_9 = 1.0$			
ρ (g cm^{-3})	1	10	10^2	10^3	1	10	10^2	10^3
Time (seconds)	55	55	55	7	50	10	1	0.5
$x(^{13}C)$.....	7×10^{-2}	4×10^{-3}	2×10^{-3}	2×10^{-4}	10^{-4}	10^{-5}	10^{-6}	10^{-8}
$x(^{15}N)$.....	750	750	1300	230	150	100	300	30
$x(^{17}O)$.....	2	20	140	160	10^{-3}	10^{-1}	10^{-1}	1
$x(^{18}O)$.....	6×10^{-3}	6×10^{-2}	4	80	10^{-3}	0.1	3	35
$x(^{19}F)$.....	5×10^{-2}	0.5	8	30	70	200	400	250
$x(^{21}Ne)$.....	100	80	100	280	50	10	5	10
$x(^{22}Ne)$.....	10	10	6	2	2	5	15	40

V. ASTROPHYSICAL IMPLICATIONS AND CONCLUSIONS

We now wish to summarize the main results of this exploratory study. As has been emphasized throughout this paper, the resulting abundance patterns are extremely sensitive to the physical conditions: time scale, density, and especially temperature. The temperature range of interest is itself well defined. For temperatures as low as $T_9 \simeq 0.1$ the results are similar to those obtained from the slow CNO cycle (Caughlan and Fowler 1962; Caughlan 1965), namely, a large abundance of ^{14}N is obtained compared to C and O, while at temperatures $T_9 \simeq 1$ all the nuclei of $A \leqslant 22$ are transformed into ^{24}Mg (or heavier nuclei perhaps if the network were extended). $T_9 = 1$ is definitively the upper limit of the range in which hot CNO-cycle burning would occur.

There are several important implications of these results for problems of nucleosynthesis.

a) For the conditions considered in these calculations (solar abundances) the neutron flux available is never sufficient to drive the standard *s*-process.

b) The transformation of hydrogen into helium occurs on time scales exceeding 2–3 $\times$ 10^4 s. The time scale for hydrogen depletion decreases with increasing temperature up to $T_9 \sim 0.5$, beyond which it increases slightly with temperature. This behavior, peculiar to CNO burning at higher temperatures, results from increased contributions from (γ, p) and (α, p) reactions at higher temperatures as described in § IV(*a*).

c) Among the nuclear species studied here, we have seen that ^{13}C production demands lower temperatures than the other isotopes. This is due in particular to the large rate of the $^{13}N(p, \gamma)^{14}O$ reaction at temperatures $T_9 \geq 0.2$. There are several promising environments for ^{13}C production: carbon and S-type stars may contribute significant amounts of ^{13}C (Scalo and Ulrich 1973; Truran 1973; Sackmann *et al.* 1973). In this regard, it is important to note that comparable relative enhancements of ^{13}C and *s*-process nuclei are observed in S-type stars. Carbon-13 may also be produced together with ^{15}N and ^{17}O in supernova or nova shells which have not been subjected to too high temperatures ($T_9 < 0.3$) (see, for instance, the calculations of Starrfield *et al.* 1972, 1973 relevant to nova explosions). Studies of hydrogen burning in explosions of supermassive stars also indicate that this isotope is overproduced in such circumstances (Audouze and Fricke 1973).

d) Significant enhancement of ^{15}N and ^{17}O occurs at temperatures T_9 from 0.2 to 0.5. Lesser enhancements of mass 18, 19, and 21 also occurred in some circumstances, but these are particularly sensitive to the time scale. This is due to the fact that the

positron-decay progenitors are very short lived: the half-lives of ^{18}Ne, ^{19}Ne, and ^{21}Na are respectively 1.5, 18, and 21 s. Furthermore, these progenitors (especially ^{18}Ne and ^{19}Ne) are only produced in significant amounts at high temperature ($T_9 > 0.5$) [^{18}Ne is produced mainly by ^{17}F$(p, \gamma)^{18}$Ne and ^{19}Ne by ^{15}O$(\alpha, \gamma)^{19}$Ne]. At these high temperatures ^{18}O, ^{18}F, ^{19}F, and ^{21}Ne are very rapidly destroyed by (p, α) reactions; significant production of these isotopes therefore demands that the temperature be effectively turned off on a time scale of the order of the positron-decay lifetime, placing severe restrictions on the dynamic models.

It is important to note that our predictions of abundance enhancements are sensitive in many cases to uncertainties in nuclear reaction rates. Wherever possible, we have used the nuclear rates compiled by Fowler *et al.* (1973) on the basis of existing nuclear data. Unfortunately, several critical nuclear rates which govern the production and destruction of masses $A = 17$, 18, and 19 involve unstable nuclear species, and are not available from experiment: the ^{14}O$(\alpha, p)^{17}$F, ^{15}O$(\alpha, \gamma)^{19}$Ne, ^{17}F$(p, \gamma)^{18}$Ne, and ^{18}F$(p, \alpha)^{15}$O reactions. We have adopted the estimates of these rates presented by Wagoner *et al.* (1967) and Wagoner (1969). Uncertainties in these rates may result in distortions of the relative yields at masses $A = 18$ and 19 predicted by our calculations. While the enhancement determined in these studies for ^{19}F are typically 10 times those found for ^{18}O, adjustments of these rates within the limits of uncertainty can allow predictions of comparable relative enhancements.

To conclude this preliminary study on the hot CNO–Ne cycle, it appears that the nuclei from ^{12}C up to ^{25}Mg must have a complex nucleosynthesis history. To account for the observed abundances, several different processes may or must have occurred, including helium burning in nonexplosive stars to account for ^{12}C, ^{16}O, and ^{22}Ne (Deinzer and Salpeter 1964; Vidal, Shaviv, and Kozlovsky 1971; Couch and Arnett 1972); explosive carbon burning to account for ^{20}Ne, ^{23}Na, ^{24}Mg, and ^{25}Mg (Arnett 1969); the CNO–Ne cycle at various temperatures, low T for ^{13}C and ^{14}N (Caughlan and Fowler 1962; Caughlan 1965), intermediate T for ^{15}N, ^{17}O, and ^{21}Ne, high T for ^{18}O, ^{19}F, and ^{22}Ne; possibly explosive helium burning for ^{15}N, ^{18}O, ^{19}F, and ^{21}Ne (Howard, Arnett, and Clayton 1971), and finally the still mysterious spallation processes (Audouze 1970) in supernovae (Colgate 1973) or in supermassive-star envelopes (Hoyle and Fowler 1973). It is the task of forthcoming works to define a possibly simpler account of the nucleosynthesis regarding this important region of the Mendeleev table.

One of us (J. A.) was supported by a U.S.–French exchange NSF-CNRS fellowship during the preparation of this paper. We thank Drs. A. G. W. Cameron, William A. Fowler, R. T. Rood, J. Silk, R. L. Smith, and S. Starrfield for useful conversations at various stages of the work. We also thank Drs. G. R. Caughlan and William A. Fowler for communicating the results of their calculations to us prior to publication. Part of the calculations were done on the CDC 7600 located at the Lawrence Berkeley Laboratory. Two of us (J. A. and J. W. T.) also wish to thank Dr. R. Jastrow for the hospitality at the Goddard Institute for Space Studies (New York) where a large part of the computations were carried out.

APPENDIX

NUCLEAR PROCESSING OF MATTER OF DIFFERENT INITIAL COMPOSITION

The preceding analysis is based upon calculations performed for matter of solar-system composition. In order to illustrate the effects of variations in the initial

composition, calculations have been performed for $T_9 = 0.2$, 0.5, and 1 and $\rho = 100$ g cm^{-3} for the following cases:

Composition A: $X(\mathrm{H}) = 0.74$, $X(^4\mathrm{He}) = 0.24$, $X(^{12}\mathrm{C}) = X(^{16}\mathrm{O}) = 0.01$.

Composition B: $X(\mathrm{H}) = 0.68$, $X(^4\mathrm{He}) = 0.22$, $X(^{12}\mathrm{C}) = X(^{16}\mathrm{O}) = 0.05$.

TABLE 8

RESULTS OF THE CHEMICAL EVOLUTION OF MATTER WITH DIFFERENT INITIAL COMPOSITIONS
[Composition A: $X(\mathrm{H}) = 0.74$, $X(^4\mathrm{He}) = 0.24$, $X(^{12}\mathrm{C}) = X(^{16}\mathrm{O}) = 0.01$;
Composition B: $X(\mathrm{H}) = 0.68$, $X(^4\mathrm{He}) = 0.22$, $X(^{12}\mathrm{C}) = \mathrm{X}(^{16}\mathrm{O}) = 0.05$]

Element	Time (s)	Solar-System Abundance	$T_9 = 0.2$		$T_9 = 0.5$		$T_9 = 1$	
			Comp. A	Comp. B	Comp. A	Comp. B	Comp. A	Comp. B
^{12}C....	5	4.6(−3)	0.13	0.81	...	...	...	...
	60		1.0(−2)	5.4(−2)	...	2.8(−5)	...	...
	500		2.6(−2)	0.15	1.0(−5)	5.2(−5)	...	...
^{13}C....	5	4.6(−5)	1.1(+2)	5.7(+2)	1.3(−4)	6.8(−4)	...	...
	60		2.6	14	1.1(−3)	5.6(−3)	...	...
	500		7.6	44	2.0(−3)	1.1(−2)	...	...
^{14}N...	5	9.7(−4)	5.8	26	11	57	...	4.7(−5)
	60		7.7	37	6.8	34	...	2.0(−5)
	500		7.3	35	5.7	28	...	...
^{15}N...	5	3.8(−6)	26	1.2(+2)	2.2(+2)	1.1(+3)	13	71
	60		1.4(+3)	6.9(+6)	1.9(+3)	9.0(+3)	3.7	26
	500		3.4(+3)	1.7(+4)	3.4(+3)	1.6(+4)	4.0(−4)	1.4(−2)
^{16}O....	5	1.0(−2)	0.94	4.7	0.91	4.6	2.0	10
	60		0.52	2.8	0.75	3.9	0.51	3.3
	500		7.7(−3)	6.5(−2)	0.29	1.9	5.9(−5)	1.7(−3)
^{17}O....	5	4.3(−6)	1.4(+2)	6.3(+2)	1.8(+2)	8.1(+2)	0.13	0.60
	60		8.9(+2)	4.2(+3)	1.4(+2)	6.7(+2)	3.2(−2)	0.19
	500		9.0(+1)	5.5(+2)	56	3.0(+2)	...	9.3(−5)
^{18}O....	5	2.5(−5)	2.0(−5)	9.6(−5)	4.4	19	3.8	18
	60		3.6(−4)	1.8(−3)	4.0	17	0.96	6.0
	500		4.0(−5)	2.8(−4)	1.5	7.2	1.1(−4)	2.8(−3)
^{19}F....	5	2.0(−6)	...	1.4(−4)	0.27	1.2	46	2.2(+2)
	60		5.0(−3)	2.5(−2)	11	47	18	1.3(+2)
	500		1.1(−3)	6.0(−3)	27	1.4(+2)	1.9(−3)	6.5(−2)
^{20}Ne...	5	1.2(−3)	...	...	...	...	...	...
	60		...	...	7.9(−4)	3.2(−3)	...	1.7(−5)
	500		...	...	4.2(−3)	1.8(−2)	...	...
^{21}Ne...	5	3.6(−6)	...	...	7.8(−2)	0.33	6.7	31
	60		...	...	0.47	2.1	1.9	11
	500		...	...	2.8	12	2.2(−4)	5.5(−3)
^{22}Ne...	5	1.3(−4)	...	...	2.0(−4)	8.5(−4)	18	72
	60		...	...	1.0(−2)	4.6(−2)	10	49
	500		...	...	0.11	0.52	1.0(−3)	2.3(−2)
^{23}Na..	5	4.2(−5)	...	...	2.6(−5)	3.1(−4)	11	48
	60		...	...	9.5(−3)	3.8(−2)	14	76
	500		...	...	0.13	0.57	1.3(−3)	3.6(−3)
^{24}Mg..	5	5.7(−4)	...	...	...	...	1.8	7.0
	60		...	...	2.1(−4)	8.3(−3)	44	1.9(+2)
	500		...	...	3.3(−2)	0.14	61	3.2(+2)
^{25}Mg..	5	7.6(−5)	...	...	...	...	3.9(−3)	1.6(−2)
	60		...	...	...	...	7.5(−2)	0.32
	500		...	...	...	4.8(−5)	0.10	0.46

NOTE.—Calculations have been made for $T_9 = 0.2$, 0.5, and 1; and $\rho = 100$ g cm^{-3}. The calculated enhancements or depletions factors are listed at three different times and compared with the solar mass fractions (recalled in col. [3]). Depletion factors $\times < 10^{-5}$ and mass fractions less than 10^{-10} are not reported in the table.

In both cases, the H/He ratio is that of solar-system matter, while only the total amounts of $^{12}C + {}^{16}O$ vary. The results of these calculations are summarized in table 8, where the ratios to solar-system abundances are presented for burning times 5, 60, and 500 sec (corresponding approximately to the hydrodynamic time scales for densities 10^4, 10^2, and 1 g cm^{-3}, respectively).

The results obtained here are quite similar to those described in the text: at $T_9 = 0.2$, large overabundances of ^{13}C, ^{14}N, ^{15}N, and ^{17}O are produced; at $T_9 = 0.5$, ^{12}C and ^{13}C are depleted, ^{14}N, ^{15}N, and ^{17}O are significantly enhanced and mild enhancements of ^{18}O and ^{19}F occur; for $T_9 = 1$, the bulk of the metals are ultimately transformed into ^{24}Mg, although ^{18}O, ^{19}F, and ^{22}Ne remain overabundant by factors ~ 10 after ~ 60 s. The main difference between these results and those for the solar case is that, in the absence of any initial ^{20}Ne, no significant production of ^{21}Ne occurs.

These calculations again illustrate and define the temperature range appropriate to the production of various isotopes: ^{13}C ($T_9 \lesssim 0.2$), ^{14}N ($T_9 < 0.5$), ^{15}N and ^{17}O ($0.2 \leq T_9 \leq 0.5$) ^{18}O and ^{19}F ($0.5 \leq T_9 \lesssim 1$) and ^{22}Ne ($T_9 \sim 1$).

REFERENCES

Appenzeller, I., and Fricke, K. 1972, *Astr. and Ap.*, **21**, 285.
Arnett, W. D. 1969, *Ap. J.*, **157**, 1369.
Arnett, W. D., and Truran, J. W. 1969, *Ap. J.*, **157**, 339.
Audouze, J. 1970, *Astr. and Ap.*, **8**, 436.
Audouze, J., and Fricke, K. 1973, preprint.
Bethe, H. A. 1939, *Phys. Rev.*, **55**, 103.
Cameron, A. G. W. 1968, in *Origin and Distribution of the Elements*, ed. L. H. Ahrens (Oxford and New York: Pergamon Press), p. 125.
Caughlan, G. R. 1965, *Ap. J.*, **141**, 688.
Caughlan, G. R., and Fowler, W. A. 1962, *Ap. J.*, **136**, 453.
———. 1964, *ibid.*, **139**, 1180.
———. 1972, *Nature Phys. Sci.*, **238**, 23.
———. 1973, in preparation.
Caughlan, G. R., Fowler, W. A., and Talbot, R. J. 1964, *Ap. J.*, **140**, 380.
Colgate, S. A. 1973, preprint.
Couch, R. G., and Arnett, W. D. 1972, *Ap. J.*, **178**, 771.
Deinzer, W., and Salpeter, E. E. 1964, *Ap. J.*, **140**, 499.
Fowler, W. A., Caughlan, G. R., and Zimmerman, B. A. 1973, in preparation.
Fowler, W. A., and Hoyle, F. 1964, *Ap. J. Suppl.*, No. 91, **9**, 201.
Fricke, K. 1973, private communication.
Howard, W. M., Arnett, W. D., and Clayton, D. D. 1971, *Ap. J.*, **165**, 495.
Hoyle, F., and Fowler, W. A. 1960, *Ap. J.*, **132**, 565.
———. 1965, in *Quasi-Stellar Sources and Gravitational Collapse*, ed. I. Robinson, A. Schild, and E. L. Schucking (Chicago: University of Chicago Press), p. 17.
———. 1973, *Nature*, **241**, 384.
Sackmann, I.-J., Smith, R. L., and Despain, K. 1973, preprint.
Scalo, J. M., and Ulrich, R. K. 1973, *Ap. J.*, **183**, 151.
Scarborough, J. B. 1966, *Numerical Mathematical Analysis* (6th ed.; Baltimore: Johns Hopkins Press).
Starrfield, S., Sparks, W. M., and Truran, J. W. 1973, in preparation.
Starrfield, S., Truran, J. W., Sparks, W. M., and Kutter, G. 1972, *Ap. J.*, **176**, 169.
Truran, J. W. 1973, in *Proceedings of the Conference on Red Giant Stars*, October 4–6, 1972 (Bloomington: Indiana University Press), to be published.
Vidal, N. V., Shaviv, G., and Kozlovsky, B. Z. 1971, *Astr. and Ap.*, **13**, 147.
Wagoner, R. V. 1969, *Ap. J. Suppl.*, No. 162, **18**, 247.
Wagoner, R. V., Fowler, W. A., and Hoyle, F. 1967, *Ap. J.*, **148**, 3.
Weizsäcker, C. F. von. 1938, *Physik Z.*, **39**, 633.